Infrared Physics and Technology 101 (2019) 39–44

Contents lists available at ScienceDirect

Infrared Physics & Technology

journal homepage: www.elsevier.com/locate/infrared

Regular article

Near infrared heterodyne radiometer for continuous measurements of atmospheric CO_2 column concentration

Hao Deng[a,b], Chenguang Yang[a,*], Wei Wang[a], Changgong Shan[a,b], Zhenyu Xu[a], Bing Chen[a], Lu Yao[a], Mai Hu[a,b], Ruifeng Kan[a,c,*], Yabai He[a,b]

[a] Key Laboratory of Environmental Optics and Technology, Anhui Institute of Optics and Fine Mechanics, Chinese Academy of Science, Hefei, Anhui 230031, China
[b] University of Science and Technology of China, Hefei, Anhui 230022, China
[c] Changchun Institute of Optics, Fine Mechanics and Physics, Chinese Academy of Sciences, Changchun 130033, China

ARTICLE INFO

Keywords:
Carbon dioxide
Column concentration
Laser heterodyne radiometer (LHR)
Distributed feedback (DFB) diode laser

ABSTRACT

We report a laser heterodyne radiometer (LHR) using a distributed feedback (DFB) diode laser operating in the near infrared region as the local oscillator to continuously measure atmospheric carbon dioxide (CO_2) column concentration, which has a spectral resolution of 0.09 cm^{-1}. The measurements for three consecutive days show that the averaged CO_2 column concentration are 411.5 ppm, 410.4 ppm and 409.5 ppm, respectively. The averaged measurement precision is 1.6% by analyzing the standard deviation of CO_2 column concentration. The relative error of 0.3% is estimated by comparing to CO_2 average column concentration derived from GOSAT data on October 31, 2018 during the same measurement period. Moreover, the CO_2 results are in good agreement with those measured by the ground-based Fourier transform spectrometer (FTS) simultaneously. The results prove the capacity and the reliability of the developed near infrared LHR to monitor the time series of regional CO_2.

1. Introduction

Carbon dioxide (CO_2), as the most important anthropogenic greenhouse gas, accounts for 63.5% of the total forced contribution of greenhouse gas radiation. It has stable chemical properties and a long lifetime of several decades. The main emission source of CO_2 is fossil fuel combustion, such as automobile exhaust and industrial manufacture. Over the recent decades, the mean annual column concentration of CO_2 has grown at a rate of 2.2 ppm per year according to the monitoring results of GOSAT. Therefore, it is of high importance to monitor concentration of CO_2 in the atmosphere continuously and accurately to investigate the influence of its interannual variations on regional climate change [1].

Currently, ground-based Fourier transform spectrometer (FTS) [2] with high precision is a relatively ideal instrument to observe this variation, which is used to calibrate and validate satellite datasets from GOSAT and OCO-2 data [3–5]. But, its high instrument costs and huge size for the ultrahigh spectral resolution limit its application. Instead, laser heterodyne radiometer (LHR) has been extensively applied for atmospheric measurements [6–13] and planetary observations [14–16], due to its advantage of high spectral resolution, high signal to noise ratio, ultrahigh detection sensitivity and small volume. With the development of semiconductor lasers, the quantum cascade laser (QCL) becomes the ideal mid-infrared local oscillator light source of LHR for their high optical power, narrow linewidth and wide tuning range. QCL based LHR has been used to measure the greenhouse gases in the atmosphere [6,7,9,12,13,15,17]. There are main issues still present in the QCL based LHR, such as the poor stability of photomixing because of its using free optic coupling method, and the high cost of QCL and mercury cadmium telluride detector with high performance. Instead, the distributed feedback (DFB) diode laser operating in the near infrared, InGaAs detector and fiber coupler show more competitive in terms of cost performance of product. Therefore, the near infrared LHR is suitable to measure the regional variations of greenhouse gases. A miniaturized, low cost LHR based on all fiber has been developed for atmosphere studies by the groups of Wilson et al [18–20], in which the near infrared DFB diode laser is adopted. However, there is still lack of report on continuous measurements of regional CO_2 column concentration with LHR.

In present study, we developed a near infrared LHR to measure the column concentration of CO_2 in the atmosphere based on the absorption spectra of sunlight. The determined results are obtained from the

* Corresponding authors at: Key Laboratory of Environmental Optics and Technology, Anhui Institute of Optics and Fine Mechanics, Chinese Academy of Science, Hefei, Anhui 230031, China.
E-mail addresses: cgyang@aiofm.ac.cn (C. Yang), rfkan@ciomp.ac.cn (R. Kan).

https://doi.org/10.1016/j.infrared.2019.06.002
Received 22 February 2019; Received in revised form 7 May 2019; Accepted 6 June 2019
Available online 07 June 2019
1350-4495/

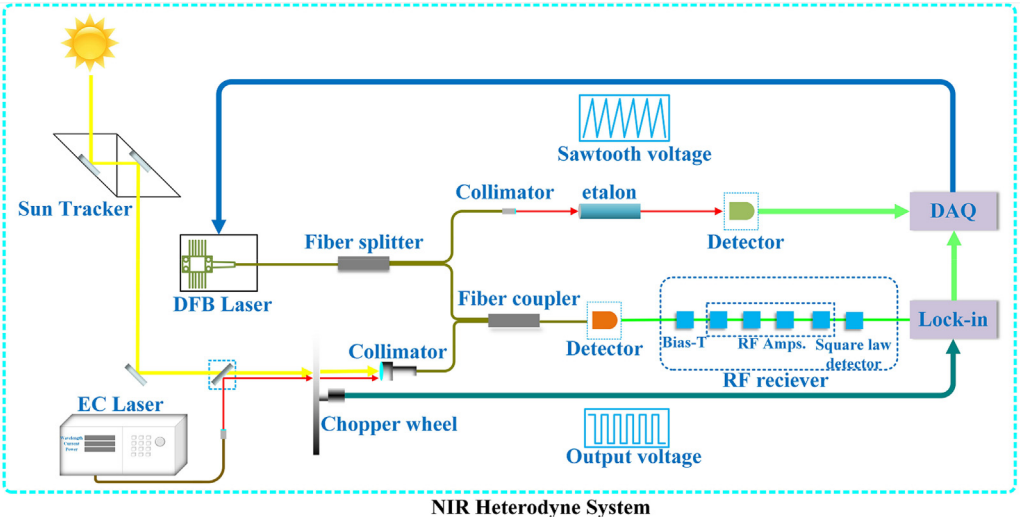

Fig. 1. The developed near infrared LHR for detection of CO_2 column concentration in the atmosphere.

developed near infrared LHR for three consecutive days. In addition, the synchronous measurement results of CO_2 achieved by the ground-based Fourier transform spectrometer (FTS) [21] in Hefei of China are used for comparison to verify the validity of the measured results.

2. Experimental details

2.1. Instrument

A schematic of the near infrared LHR used in this work is shown in Fig. 1. A sun tracker (Solar Tracker-A547, Bruker Optics) was used to collect sunlight with high tracking precision (< 0.1°). The collected sunlight was modulated by a mechanical chopper (MC2000B-EC, Thorlabs) with 750 Hz chopping frequency. Then, the sunlight was coupled into the single mode fiber by a reflection-type collimator (RC08FC-P01, Thorlabs). The numerical aperture of the collimator is equivalent to that of the single mode fiber (0.167), which means that the collimator has the ability to coupling most of the sunlight into the fiber. A DFB diode laser (NLK1L5GAAA, NEL) was utilized as the local oscillator with the optical power up to 20 mW. The wavelength of the DFB diode laser can be tuned from 1571 nm to 1573 nm by properly adjusting the laser temperature and injection current with a home-made laser temperature and current controller. The light emitted from the DFB diode laser was divided into two beams by a fiber splitter, namely the local oscillator beam and the reference beam. The local oscillator beam with 95% of the output laser power was superimposed with the collected sunlight in a single mode fiber coupler (F-CPL-F12131, Newport), and mixed in a fast detector (DET08CFC/M, Thorlabs) with the bandwidth of 5 GHz, to produce radio frequency (RF) beat signal. Then, the RF signal was filtered and amplified by a RF processing circuit. Within the RF circuit, a bias-tee was used to filter out the direct current. Then, the beat signal passed a four-stage RF amplifier. A schottky diode was applied for measuring the power of the amplified signal. The final signal was demodulated by a digital lock-in amplifier (SR865A DSP, SRS). The obtained heterodyne spectrum was acquired with a 16-bit data acquisition card (USB-6363, NI). At the same time, the reference beam passed through a quartz FP etalon. The created interference signal was detected by a InGaAs detector with 2 MHz bandwidth and acquired with the same data acquisition card. The central positions of CO_2 absorption peaks were calibrated by combining the known spectral line parameters of CO_2 extracted from HITRAN database [22]. Furthermore, the bandwidth of the near infrared LHR was calibrated with an external cavity diode laser (ECDL) (Tunics-100, Yenisita) as the signal light, the linewidth of which is less than 100 kHz. And the procedure was the same as that of measurements of CO_2 absorption spectrum of the atmosphere.

2.2. The theory of laser heterodyne spectroscopy

The principle representation of laser heterodyne detection is given in Fig. 2. Suppose that the local oscillator and the signal light are perfectly aligned plane waves, and can be represented by

$$E_{LO} = A_{LO}\cos(\omega_{LO}t + \phi) \tag{1}$$

and

$$E_s = A_s\cos(\omega_s t) \tag{2}$$

where E_{LO} and E_s are the fields of the local oscillator and the signal light, A_{LO} and A_s are amplitudes of the fields, ω_{LO} and ω_s are angle frequencies of the fields, ϕ is phase of the field of the local oscillator. The generated response current of the detector can be written as follows when the local oscillator is mixing with the source on the active area of detector.

$$i = \kappa(E_{LO} + E_S)^2 \tag{3}$$

where κ is a proportionality constant containing the detector quantum efficiency. The above equation can be expressed as

$$\begin{aligned} i &= \kappa\Big\{A_sA_{LO}\cos[(\omega_{LO}+\omega_s)t+\phi] + \frac{1}{2}A_s^2(1+\cos 2\omega_s t) \\ &\quad + \frac{1}{2}A_{LO}^2(1+\cos 2\omega_{LO}t) + A_sA_{LO}[\cos(\omega_{LO}-\omega_s)t+\phi]\Big\} \end{aligned} \tag{4}$$

Due to the bandwidth limitation of the photodetector, the high-frequency terms of $A_sA_{LO}[\cos(\omega_{LO}+\omega_s)t+\phi]$, $\frac{1}{2}A_s^2\cos 2\omega_s t$ and $\frac{1}{2}A_{LO}^2\cos 2\omega_{LO}t$, will not be responded by the detector, so it can be directly ignored. The Eq. (4) can be simplified as

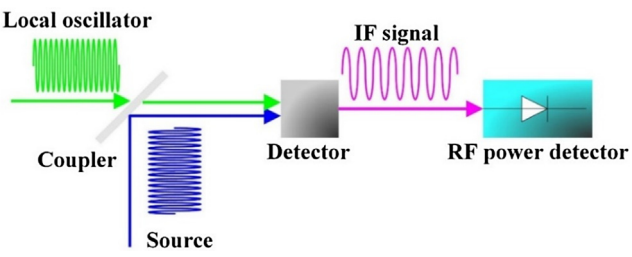

Fig. 2. Schematic representation of laser heterodyne detection.

$$i = \kappa\left\{\frac{1}{2}A_s^2 + \frac{1}{2}A_{LO}^2 + A_sA_{LO}[\cos(\omega_{LO} - \omega_s)t + \phi]\right\} \quad (5)$$

where $\frac{1}{2}A_s^2$ and $\frac{1}{2}A_{LO}^2$ are direct current (DC) terms, and $A_sA_{LO}[\cos(\omega_{LO} - \omega_s)t + \phi]$ is intermediate frequency (IF) term. In the detection process, the DC terms are generally filtered through the RF filter or band-pass filter and the IF term is retained. The difference frequency signal power can be detected by the RF power detector, and its output power$P$is proportional to the square of the difference frequency current, which can be expressed as

$$P \propto \kappa^2 A_s^2 A_{LO}^2 \quad (6)$$

The above equation can be further simplified as

$$P \propto \frac{1}{4}\kappa^2 I_S I_{LO} \quad (7)$$

where I_{LO} and I_S represent the intensities of the local oscillator and the signal light, respectively. Therefore, the broadband spectrum of blackbody radiation source, such as solar radiation, can be obtained by laser heterodyne detection. The noise analysis for laser heterodyne detection has been detailedly described in the Ref. [23].

3. Results and discussion

3.1. Measurement of spectral resolution

The CO_2 absorption spectra of the atmosphere was obtained by the LHR, as shown in Fig. 3. It can be seen that the two strong absorption of CO_2 are present in the laser scanning range, located at 6363.72756 cm^{-1} (R 22e) and 6364.92202 cm^{-1} (R 24e), respectively. The data were taken in Hefei of China located at 31.9°N, 117.2°E. The free spectral range of the interference fringe, which is also shown in Fig. 3 with red curve, is 0.0692 cm^{-1}. In order to obtain the spectral resolution of the LHR accurately, the narrow linewidth ECDL fixed at 6363.6225 $cm^{-1}$was used. Then, the DFB diode laser scanned across the target wavelength, and the heterodyne signal after photomixing between the two lasers and RF processing, was demodulated by the locking-in amplifier. Fig. 4 shows the measured heterodyne signal and the fitting results of the curve that is performed by using a nonlinear least-squares procedure and combining with a standard Gaussian profile. The spectral resolution of the LHR equals to twice the measurement linewidth of the fitting curve, 1.35 GHz (0.09 cm^{-1}) because of double-sideband detection [23].

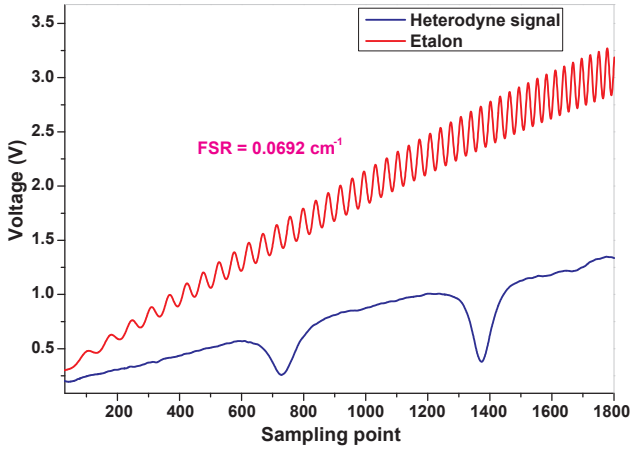

Fig. 3. Experimentally measured interference fringes by the optical etalon (red curve) and experimentally observed atmospheric CO_2 absorption spectrum by the near infrared LHR (blue curve). (For interpretation of the references to colour in this figure legend, the reader is referred to the web version of this article.)

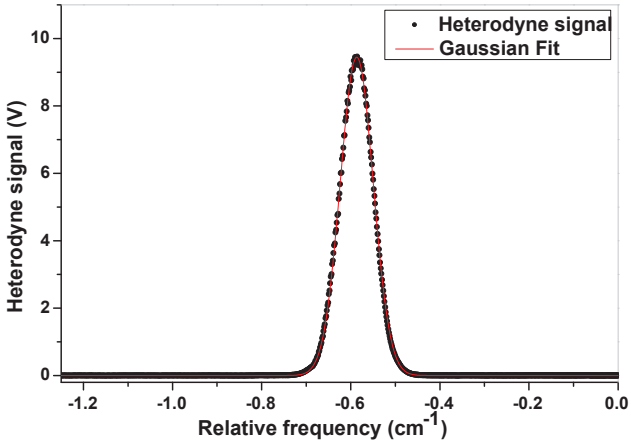

Fig. 4. The heterodyne signal obtained by mixing an external laser with fixed wavelength with the local oscillator represented by the black dots and the Gaussian fitting results represented by the red line.

3.2. Retrieval of CO_2 absorption spectra

During the experiment, we have monitored CO_2 column concentration of daytime using the LHR for three days continuously. A polynomial fitting algorithm was used to calculate the background solar radiation. The measured transmission spectra of atmospheric CO_2 with different solar altitude angles are shown in Fig. 5. The spectral signals were generally retrieved from an average of 50 scans to improve signal to noise ratio (SNR).

In order to deduce CO_2 column concentration precisely, the details of the sunlight transmission process have to be considered. The collected sunlight spectrum can be regarded as the path integration of gas absorption spectra at different altitudes, where the pressure and temperature are different. Therefore, it is necessary to divide the atmosphere into different layers to ensure the accuracy of the calculated column concentration of CO_2. In this work, the atmosphere top of the model is around 76 km. The whole atmosphere is divided into 76 layers. The atmospheric vertical profiles of pressure, temperature, and water vapor were taken from the National Centers for Environment Prediction (NCEP). A cubic spline interpolation algorithm (CSIA) was used to resolve the parameters of different layers with respect to temperature and pressure. An algorithm for retrieval of the column concentration of CO_2 was programmed in Python based on a nonlinear least square method, the Line-By-Line Radiative Transfer Model (LBLRTM) [24,25], and HITRAN database as input [22]. It can be simply written as follows

$$T = \exp(-\alpha_{total}) = \exp\left(-\sum_{j=1}^{M}\sum_{i=1}^{N}\alpha_{ji}\right) = \exp\left(-\sum_{j=1}^{M}\sum_{i=1}^{N}s_{ji}\cdot\sigma_{ji}\cdot n_{ji}\cdot l_j\cdot\bar{c}\right) \quad (8)$$

where T is the transmission, α_{total} is the total absorbance, α_{ji} is the absorbance of the i_{th} absorption line of the j_{th} layer, s_{ji} is the line strength of the i_{th} absorption line of the j_{th} layer, σ_{ji} is the cross section of the i_{th} absorption line of the j_{th} layer, n_{ji} is the number density of molecules of the i_{th} absorption line of the j_{th} layer, l_j is the altitude of the j_{th} layer, and $\bar{c}$ is the vertical column concentration of target molecule. In addition, the standard Voigt profile function was adopted, and the spectral resolution of the LHR was taken in account as well, which is considered as the convolution with Lorenz profile. The spectral fitting results are also presented in Fig. 5, and the residuals calculated are less than 0.02, which illustrates the accuracy of the retrieved CO_2 column concentration. The CO_2 column concentrations can be calculated by the developed retrieval algorithm, corresponding to 408.4 parts per million (ppm), 410.1 ppm, and 413 ppm, respectively. The average SNR of spectral signals is calculated by the ratio of the absorption depth to the

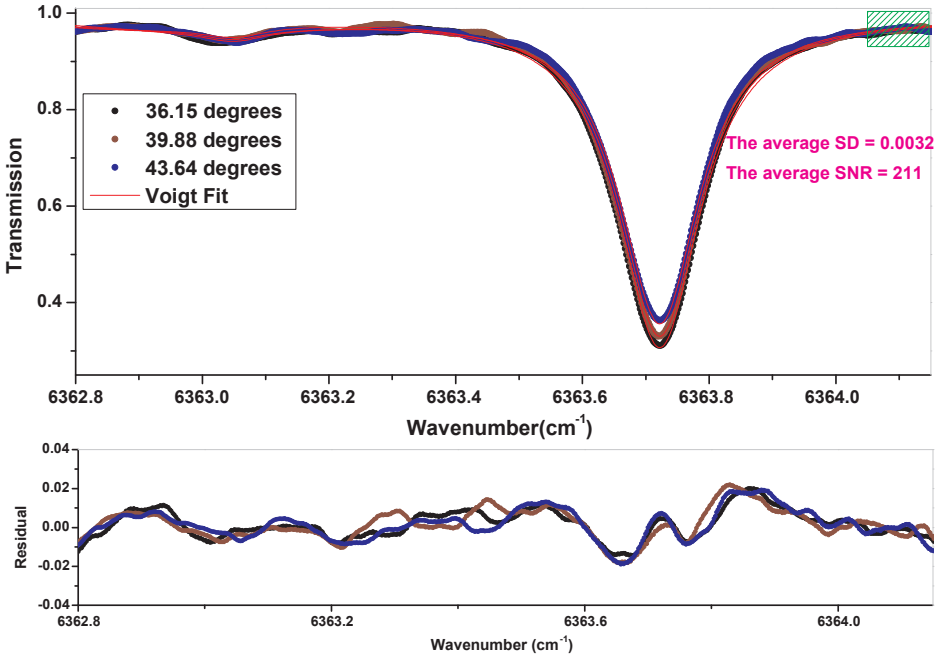

Fig. 5. The measured CO_2 absorption spectra with different solar altitude angles and their Voigt fitting curves shown in the upper panel, and the corresponding residuals shown in the bottom panel.

standard deviation of baseline marked by the green shadow, and is about 211. It means that a minimum detection limit of 1.9 ppm for CO_2 can be obtained when SNR = 1. The minimum detection limit can be further improved by increasing the integration time or the collimator size to enhance the SNR of heterodyne signal.

3.3. CO_2 column concentration observations and comparison with the data of ground-based FTS

Ground-based FTS has been proved to be a powerful tool for regional CO_2 column concentration measurement for the reason of its high resolution and ultrahigh measurement precision. Thus, the performance of our developed LHR can be better evaluated by comparing with the ground-based FTS data, such as spectral signals and CO_2 column concentration observation results. In this work, CO_2 column concentration were measured simultaneously by the LHR and the ground-based FTS [21] in Hefei of China in the same location. The atmospheric CO_2 transmitted spectra, obtained by the LHR and the ground-based FTS, respectively, has been shown in Fig. 6. The corresponding solar altitude angle is approximately 35 degrees. The standard deviations for the baselines marked by green shadow are figured out to be 0.0042 and 0.0027 corresponding to the ground-based FTS spectrum and the LHR spectrum, respectively. It indicates that the LHR possess a better property in terms of noise levels. Moreover, it can be found that the CO_2 transmitted spectrum obtained from the ground-based FTS is close to saturation under this solar altitude angle, while that derived from the LHR is not saturated superficially due to its lower resolution.

Therefore, we just show the observed CO_2 column concentration of nearly three hours from 11:10 am to 13:50 pm of three consecutive days on October 31, November 1, and November 2, 2018, respectively, as displayed in Fig. 7. The observed results from this figure show that atmospheric CO_2 column concentration during this period remains stable. Through calculation, the variation trend of CO_2 mean column concentrations for the three days are 411.5 ppm, 410.4 ppm and 409.5 ppm, respectively, while the corresponding standard deviations are 6.1 ppm, 6.5 ppm and 6.7 ppm. Thus, the average measurement error for the LHR is approximately 1.6%, which may be mainly caused by the variation of earth atmospheric pressure and temperature.

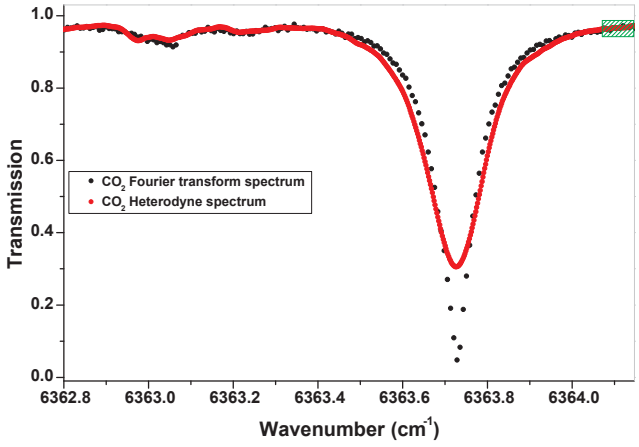

Fig. 6. The atmospheric CO_2 transmitted spectra separately measured by the LHR (red dots) and the ground-based FTS [21] (black dots). (For interpretation of the references to colour in this figure legend, the reader is referred to the web version of this article.)

Furthermore, a relative error of 0.3% has been estimated by comparing with CO_2 average column concentration in Hefei obtained from the observation results of GOSAT on November 2, 2018 during the same measurement period.

The observed CO_2 column concentration from the ground-based FTS [21] on October 31 and November 2, 2018 are present in Fig. 8, where the corresponding average column concentration of CO_2 are figured out to be 412 ppm and 409.6 ppm, respectively, and Universal Time Coordinated plus 8 h (UTC + 8), is used to represent the measurement time. It can be obviously found that the variation tendency of CO_2 column concentration is generally stable, which is the same as the observed results shown in Fig. 7. The calculated standard deviations are severally 0.8 ppm and 0.5 ppm, as demonstrates the excellent measurement precision of the ground-based FTS. Thus, the relative measurement errors of the LHR are 0.1% and 0.02%, respectively, by comparing with the retrieval of atmospheric CO_2 column concentration obtained from the ground-based FTS. Moreover, the FTS can achieve

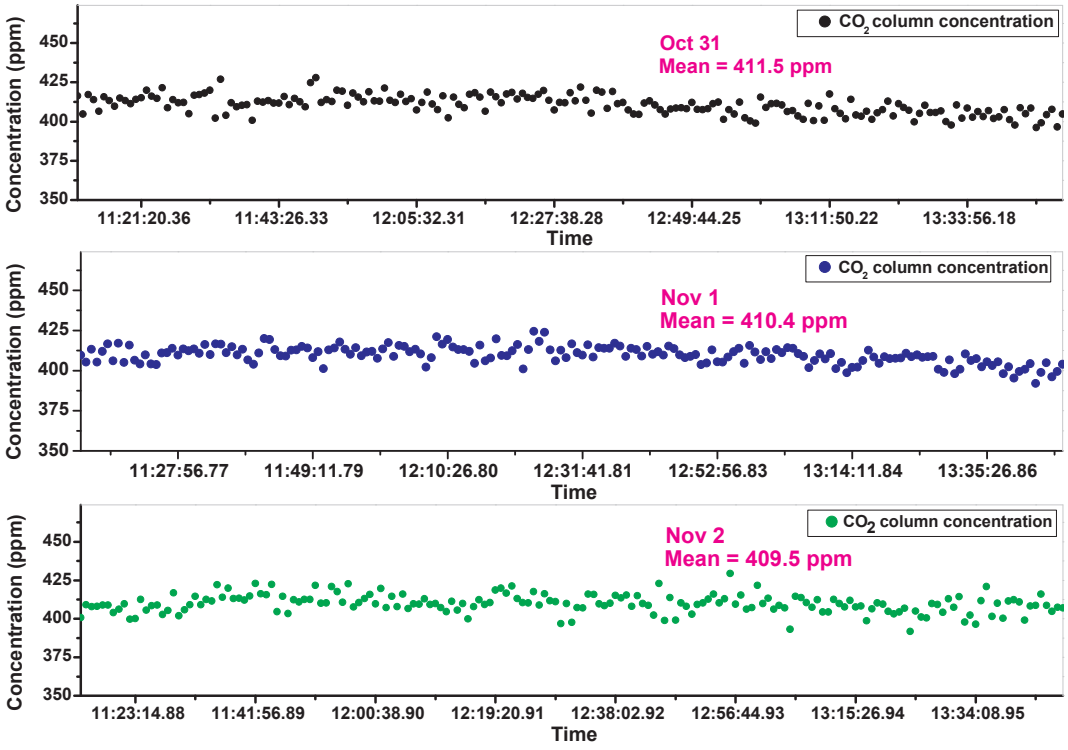

Fig. 7. The calculated CO_2 column concentration for three consecutive days.

longer time measurement because of its ability of wideband detection, while it can also be implemented by the LHR based multiple lasers or ECDL. Overall, the performance of the ground-based FTS is superior to that of our developed LHR. But the LHR has more advantages in its low cost and portability. Although the spectral resolution is lower than that of other near infrared LHR [26,27], it can meet the requirements of CO_2 column concentration measurement. Therefore, the LHR has a wide application prospect in monitoring regional variations of greenhouse gases.

4. Conclusion

In this paper, a near infrared all-fiber structure LHR with a spectral resolution of 0.09 cm^{-1} was developed for measurement of CO_2 column

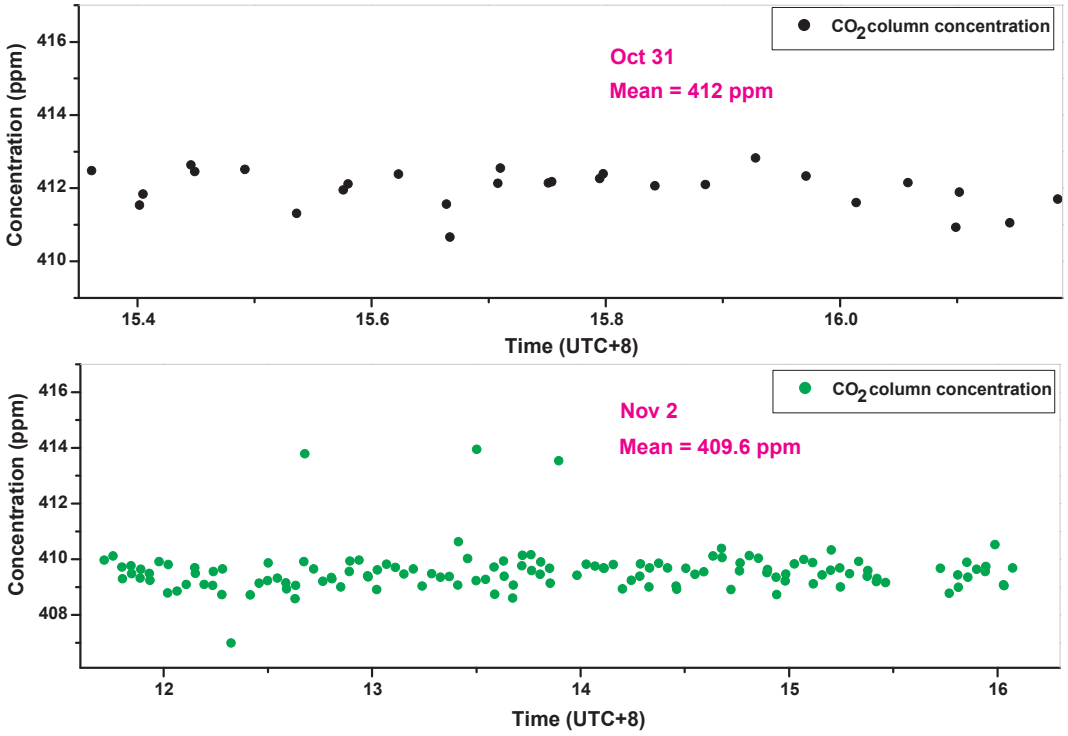

Fig. 8. Simultaneously measured CO_2 column concentration by the ground based FTS [21] for October 31 and November 2, 2018.

concentration in the atmosphere. The variation of CO_2 column concentration was continuously monitored from October 31, 2018 to November 2, 2018. The average column concentrations of CO_2 for three days are 411.5 ppm, 410.4 ppm and 409.5 ppm, respectively. And the average measurements precision for this system is estimated to be about 1.6% based on the standard deviation of the measured column concentration of CO_2. The relative error of 0.3% is achieved by comparing the CO_2 average column concentration in Hefei with that obtained from the GOSAT results during the same measurement period. In addition, the comparison of the measured results between our developed near infrared LHR and the ground-based FTS [21] in Hefei of China shows a good agreement. In the future, we will focus on performance improvement of the LHR, including increase of spectral resolution by reducing the bandwidth of the RF processing circuit, improvement of SNR of heterodyne signal by optimizing the integration time or increasing the collimator size, further enhancement of measurement precision of the LHR by simultaneously measuring oxygen column amount in the atmosphere to remove the influence of the variation of earth atmospheric pressure and temperature, and detection of atmospheric multicomponent gas by using a ECDL or multiple lasers.

Declaration of Competing Interest

Author declares that there is no conflict of interest.

Acknowledgements

This work was supported in part by the National Key Research and Development Program of China (Grant No. 2016YFC0201103 and 2016YFC1400604).

Appendix A. Supplementary material

Supplementary data to this article can be found online at https://doi.org/10.1016/j.infrared.2019.06.002.

References

[1] S. Van der Laan, R.E.M. Neubert, H.A.J. Meijer, A single gas chromatograph for accurate atmospheric mixing ratio measurements of CO_2, CH_4, N_2O, SF_6 and CO, Atmos. Meas. Tech. 2 (2) (2009) 549–559.
[2] C.P. Rinsland, N.B. Jones, B.J. Connor, J.A. Logan, P. Demoulin, Northern and Southern Hemisphere ground-based infrared spectroscopic measurements of tropospheric carbon monoxide and ethane, J. Geophys. Res. Atmos. 103 (D21) (1998) 28197–28217.
[3] S. Basu, M. Krol, A. Butz, C. Clerbaux, Y. Sawa, T. Machida, H. Matsueda, C. Frankenberg, O.P. Hasekamp, I. Aben, The seasonal variation of the CO_2 flux over Tropical Asia estimated from GOSAT, CONTRAIL, and IASI, Geophys. Res. Lett. 41 (5) (2014) 1809–1815.
[4] A. Chatterjee, R.J. Engelen, S.R. Kawa, C. Sweeney, A.M. Michalak, Background error covariance estimation for atmospheric CO_2 data assimilation, J. Geophys. Res. Atmos. 118 (17) (2013) 10140–10154.
[5] S. Guerlet, S. Basu, A. Butz, M. Krol, P. Hahne, S. Houweling, O.P. Hasekamp, I. Aben, Reduced carbon uptake during the 2010 Northern Hemisphere summer from GOSAT, Geophys. Res. Lett. 40 (10) (2013) 2378–2383.
[6] D. Weidmann, W.J. Reburn, K.M. Smith, Ground-based prototype quantum cascade laser heterodyne radiometer for atmospheric studies, Rev. Sci. Instrum. 78 (7) (2007) 073107.
[7] D. Weidmann, G. Wysocki, High-resolution broadband (> 100 cm^{-1}) infrared heterodyne spectro-radiometry using an external cavity quantum cascade laser, Opt. Exp. 17 (1) (2009) 248–259.
[8] E.L. Wilson, M.L. McLinden, J.H. Miller, G.R. Allan, L.E. Ott, H.R. Melroy, G.B. Clarke, Miniaturized laser heterodyne radiometer for measurements of CO_2 in the atmospheric column, Appl. Phys. B. 114 (3) (2014) 385–393.
[9] D. Weidmann, B.J. Perrett, N.A. Macleod, R.M. Jenkins, Hollow waveguide photomixing for quantum cascade laser heterodyne spectro-radiometry, Opt. Exp. 19 (10) (2011) 9074–9085.
[10] S.R. King, D.T. Hodges, T.S. Hartwick, D.H. Barker, High-resolution atmospheric-transmission measurement using a laser heterodyne radiometer, Appl. Opt. 12 (6) (1973) 1106–1107.
[11] R.T. Ku, D.L. Spears, High-sensitivity infrared heterodyne radiometer using a tunable-diode-laser local oscillator, Opt. Lett. 1 (3) (1997) 84–86.
[12] A. Hoffmann, N.A. Macleod, M. Huebner, D. Weidmann, Thermal infrared laser heterodyne spectroradiometry for solar occultation atmospheric CO_2 measurements, Atmos. Meas. Tech. 9 (12) (2016) 5975.
[13] A. Hoffmann, M. Huebner, N. Macleod, D. Weidmann, Spectrally resolved thermal emission of atmospheric gases measured by laser heterodyne spectrometry, Opt. Lett. 43 (16) (2018) 3810–3813.
[14] G. Sonnabend, D. Wirtz, V. Vetterle, R. Schieder, High-resolution observations of Martian non-thermal CO_2 emission near 10 um with a new tunable heterodyne receiver, Astron. Astrophys. 435 (3) (2005) 1181–1184.
[15] H. Nakagawa, S. Aoki, H. Sagawa, Y. Kasaba, I. Murata, G. Sonnabend, M. Sornig, S. Okano, J.R. Kuhn, J.M. Ritter, M. Kagitani, T. Sakanoi, M. Taguchi, M. Kagitani, IR heterodyne spectrometer MILAHI for continuous monitoring observatory of Martian and Venusian atmospheres at Mt. Haleakalā, Hawaii, Planet. Space. Sci. 126 (2016) 34–48.
[16] H. Rothermel, H.U. Käufl, Y. Yu, A heterodyne spectrometer for astronomical measurements at 10 micrometers, Astron. Astrophys. 126 (1983) 387–392.
[17] D. Weidmann, A. Hoffmann, N. Macleod, K. Middleton, J. Kurtz, S. Barraclough, D. Griffin, The methane isotopologues by solar occultation (MISO) nanosatellite mission: spectral channel optimization and early performance analysis, Remote. Sens. 9 (10) (2017) 1073.
[18] H.R. Melroy, E.L. Wilson, G.B. Clarke, L.E. Ott, J. Mao, A.K. Ramanathan, M.L. McLinden, Autonomous field measurements of CO_2 in the atmospheric column with the miniaturized laser heterodyne radiometer (Mini-LHR), Appl. Phys. B. 120 (4) (2015) 609–615.
[19] E.L. Wilson, A.J. DiGregorio, V.J. Riot, M.S. Ammons, W.W. Bruner, D. Carter, J.P. Mao, A. Ramanathan, S.E. Strahan, L.D. Oman, C. Hoffman, R.M. Garner, A 4 U laser heterodyne radiometer for methane (CH_4) and carbon dioxide (CO_2) measurements from an occultation-viewing CubeSat, Meas. Sci. Technol. 28 (3) (2017) 035902.
[20] G.B. Clarke, E.L. Wilson, J.H. Miller, H.R. Melroy, Uncertainty analysis for the miniaturized laser heterodyne radiometer (mini-LHR) for the measurement of carbon dioxide in the atmospheric column, Meas. Sci. Technol. 25 (5) (2014) 055204.
[21] W. Wang, Y. Tian, C. Liu, Y.W. Sun, W.Q. Liu, P.H. Xie, J.G. Liu, J. Xu, I. Morino, V.A. Velazco, D.W.T. Griffith, J. Notholt, T. Warneke, Investigating the performance of a greenhouse gas observatory in Hefei, China, Atmos. Meas. Tech. 10 (7) (2017) 2627–2643.
[22] L.S. Rothman, I.E. Gordon, Y. Babikov, A. Barbe, D.C. Benner, P.F. Bernath, M. Birk, L. Bizzocchi, V. Boudon, L.R. Brown, A. Campargue, K. Chance, L.H. Coudert, V.M. Devi, B.J. Drouin, A. Fayt, J.M. Flaud, R.R. Gamache, J. Harrison, J.M. Hartmann, C. Hill, J.T. Hodges, D. Jacquemart, A. Jolly, J. Lamouroux, R.J. LeRoy, G. Li, D. Long, C.J. Mackie, S.T. Massie, S. Mikhailenko, H.S.P. Müller, O.V. Naumenko, A.V. Nikitin, J. Orphal, V.I. Perevalov, A. Perrin, E.R. Polovtseva, C. Richard, M.A.H. Smith, E. Starikova, K. Sung, S.A. Tashkun, J. Tennyson, G.C. Toon, V.G. Tyuterev, G. Wagner, J. Quant. Spectrosc. Radiat. Transf. 130 (2013) 4–50.
[23] B. Parvitte, V. Zeninari, C. Thiebeaux, D. Courtois, Infrared laser heterodyne systems, Spectrochim. Acta. A. 60 (5) (2004) 1193–1213.
[24] S.A. Clough, M.J. Iacono, J.L. Moncet, Line-by-line calculations of atmospheric fluxes and cooling rates: application to water vapor, J. Geophys. Res. Atmos. 97 (D14) (1992) 15761–15785.
[25] S.A. Clough, M.J. Iacono, Line-by-line calculation of atmospheric fluxes and cooling rates: 2. Application to carbon dioxide, ozone, methane, nitrous oxide and the halocarbons, J. Geophys. Res. Atmos. 100 (D8) (1995) 16519–16535.
[26] A. Rodin, A. Klimchuk, A. Nadezhdinskiy, D. Churbanov, M. Spiridonov, High resolution heterodyne spectroscopy of the atmospheric methane NIR absorption, Opt. Exp. 22 (11) (2014) 13825–13834.
[27] J. Kurtz, S. O'Byrne, Multiple receivers in a high-resolution near-infrared heterodyne spectrometer, Opt. Exp. 24 (21) (2016) 23838–23848.